Tellus (1987), *39A*, 49–60

Intra-seasonal variability of rainfall and atmospheric energetics over northeast Brazil during the rainy season of 1979

By DHIRENDRA N. SIKDAR and JAMES B. ELSNER, *Atmospheric Sciences Division, Department of Geological/Geophysical Sciences, University of Wisconsin-Milwaukee, Milwaukee, WI 53201, USA*

(Manuscript received September 16, 1985; in final form March 18, 1986)

ABSTRACT

As an extension to recent studies concerning interannual and seasonal variability of rainfall over northeast Brazil, this study looks at the atmosphere immediately over northeast Brazil on a daily basis. Intra-seasonal variability of rainfall, winds and thermodynamic energies are examined for the wet season (February through May) of 1979. A trend is observed in the temporal rainfall pattern, from short duration showers in the early season to longer and more vigorous systems in the later season. May is noted as a transitional month between the wet and dry seasons. Circulation changes associated with rainy days include an upper-level trough extending further northward, weakened low-level easterlies and an increased moist energy flux from the north. These findings agree well with earlier investigations.

1. Introduction

The climate of interior northeast Brazil is problematic. Consecutive years may be marked with adequate rains and good harvests. During other years rain is scarce and crops do not grow. The rains occur principally during the months of February through May.

Recently, there have been a number of studies concerning the climate variability of this region. Much of the work has been in the area of interannual rainfall variability as related to large-scale circulation patterns. To depict mechanisms of rainfall fluctuation, the departure patterns of sea level pressure (SLP), wind and sea surface temperature (SST) over the tropical Atlantic were investigated for composites of extremly dry and extremely wet years (Hastenrath and Heller, 1977). Drought years were noted by a far northerly position of the equatorial trough, and by the anomalously warm water in the North Atlantic and cold water south of the equator.

The effect of southern hemispheric midlatitude fronts on rainfall over northeast Brazil has been studied by Kousky (1979, 1985). Findings indicate that fronts or their remains which penetrate the region enhance precipitation even as far north as the province of Ceara which is located along the north coast of northeast Brazil.

Moura and Shukla (1981) conducted an experiment with the GLAS General Circulation Model, using a SST anomaly pattern similar to that found by Hastenrath and Heller. They concluded that the occurrence of a warm anomaly in the North Atlantic and cold anomaly in the South Atlantic is conducive to a thermally direct meridional circulation, resulting in subsidence and reduced rainfall over northeast Brazil.

Marques et al. (1983) studied the interannual and seasonal variations in the atmosphere immediately over northeast Brazil. They found that the vertical structure of moist static energy during wet periods was similar to the structure in the equatorial trough. They also showed that during wet periods, the lower-tropospheric easterlies were comparatively weak, indicating the proximity of the equatorial trough to the region. From this it was suggested that rainfall variations in northeast Brazil are not of local origin but appear to be connected with variations of the tropical general circulation.

As a natural extension to these studies, this

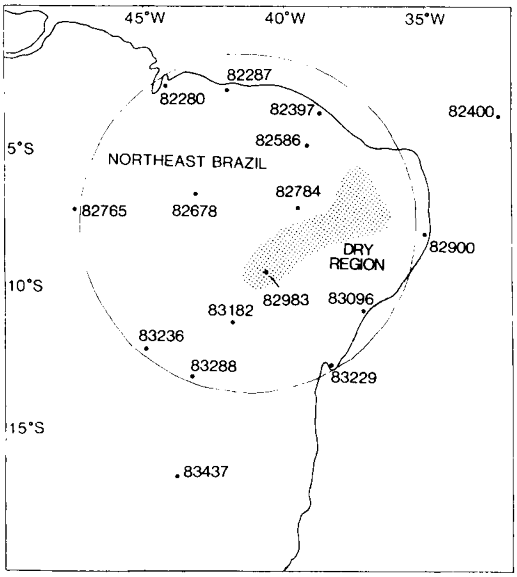

Fig. 1. Regional map of northeast Brazil with sounding station locations and dry region shaded. Perimeter of the cylinder base is depicted.

work investigates the atmosphere over northeast Brazil on a daily basis. We studied daily rainfall, as well as the structure and energetics of the atmosphere, during the rainy season of 1979, with an emphasis on variations between wet and dry days. Specifically, we used a rainfall index on daily rainfall data, and following Marques et al. (1983) we developed a cylindrical grid whose base covers most of northeast Brazil. The grid was used in computation of energy fluxes.

2. Region and data sources

We used a cylinder covering most of northeast Brazil, with 16 aerological stations within or immediately outside the circular base (Fig. 1). The cylinder was chosen to facilitate comparisons with interannual and seasonal variability and to aid in the flux computations. The cylinder base encloses the annual minimum-precipitation region (shown as the stippled area in Fig. 1) for the period 1931–1960 as computed by Strang (1972) and as appeared in Ramos (1975). The stippled area receives on the average less than 500 mm of rain per year, most of which occurs during February through May. The major hydrological concern of the region, however, is not the annual mean but rather the variability of the yearly rainfall. The area of the base circle is approximately $1{\cdot}5 \times 10^6$ km^2 and the height extends to 100 mb.

Data from the 16 aerological stations were obtained from the National Climatic Data Center in Asheville, North Carolina. Data were available for each station either at both 0000 and 1200 GMT or just 1200 GMT for February through May 1979. Components include geopotential heights, pressures, air temperature, relative humidity and the speed and direction of the wind at mandatory and significant levels. Data were composited at each station after removal of erroneous values. Since over 75% of these data were from 1200 GMT, only 1200 GMT data were used in the composites. Compositing was done at 1000, 850, 700, 500, 400, 300, 250, 200, 150 and 100 mb levels. Composite profiles were smoothed by removing data exhibiting large variance. This smoothing should lessen the effects of random errors inherent in all aerological data including the winds. The aerological winds are used for computation of both normal velocities (Section 6) and energy fluxes (Section 7). Wind errors are considered in these sections. Geopotential heights were computed from temperature profiles and compared with observed composite values. Only minor differences were noted, hence the observed values are used. Potential temperature lapse rates were found to be stable.

As a supplement to the aerological information, we used FGGE-level IIIb data grids for the area over Brazil and the tropical Atlantic sector from 30° N to 30° S. This data set was available to us only for the months of March and April. The primary element of interest from these data is zonal wind. Grid spacing is 1·875 lat-long, and vertical levels include mandatory levels up to 150 mb inclusive.

% bright cloud amounts are also used in the present study. Cloud amounts are estimated in 5° lat-long areas from infrared full disk GOES pictures, for three times daily at 0000, 1200 and 1800 GMT from February through April. The estimating procedure excludes cloudiness which appears dull gray to the eye. Cloud amounts are averaged to obtain daily means before being used in the composites.

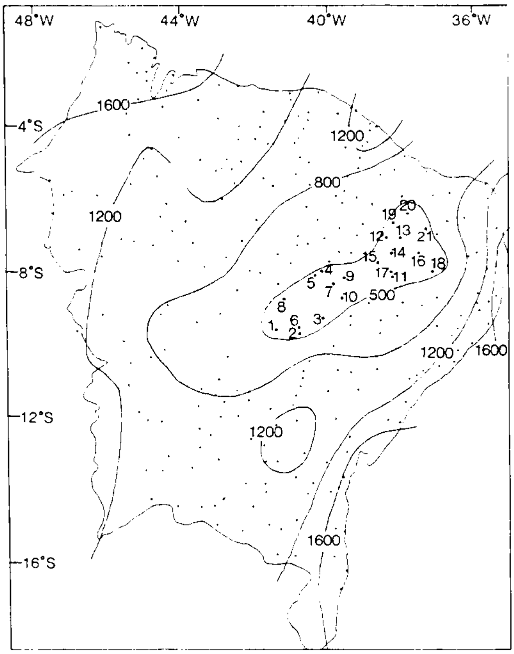

Fig. 2. Mean annual isohyets over northeast Brazil. Units are mm/yr. Analysis is from Strang (1972). Stations used in the rainfall index are numbered as follows; (1) Casa Nova, (2) Juazeiro, (3) Curaca, (4) Bodoco, (5) Ouricori, (6) Petrolina, (7) Parnamirim, (8) Afranio, (9) Serrita, (10) Cabrobo, (11) Flores, (12) Souza, (13) Pombal, (14) Itaporanga, (15) Conceicao, (16) Teixeiro, (17) Princesa Isabel, (18) Sume, (19) Alexandria, (20) Patu, (21) Caico.

Table 1. *Rainfall station list*

Number station	Latitude (S)	Longtitude (W)	Altitude (m)
1. Casa Nova	08°46′	41°14′	532
2. Juazeiro	09°05′	40°06′	350
3. Curaca	08°48′	39°40′	336
4. Bodoco	07°32′	40°06′	605
5. Ouricuri	07°50′	40°20′	444
6. Petrolina	08°25′	40°47′	500
7. Parnamirim	08°11′	40°03′	400
8. Afranio	08°38′	41°09′	630
9. Serrita	07°49′	39°29′	440
10. Cabrobo	08°19′	39°37′	550
11. Flores	08°04′	37°51′	561
12. Souza	06°37′	38°20′	420
13. Pombal	06°58′	37°47′	400
14. Itaporanga	07°18′	38°10′	230
15. Conceicao	07°21′	38°22′	470
16. Teixeiro	07°13′	37°16′	770
17. Princesa Isabel	07°44′	38°01′	660
18. Sume	07°31′	36°58′	700
19. Alexandria	06°25′	38°01′	315
20. Patu	06°06′	37°38′	305
21. Caico	06°40′	37°01′	190

For the purpose of analysis and compositing, rainfall data were obtained from the Superintendencia de Desenvolvimento do Nordeste in Recife, Pernambuco, Brazil. Data included daily totals for the entire year of 1979 from more than a thousand stations in northeast Brazil. 21 stations were chosen in the "dry region" (stippled region of Fig. 1) for use in this study. Elevations of stations ranged from 190 m at Caico, Rio Grande do Norte, to 770 m at Teixeira, Paraiba. Rainfall station locations are shown in Fig. 2, along with the mean annual isohyets computed by Strang (1972).

3. Rainfall analysis

The rainy season over much of northeast Brazil consists primarily of the months February through May and occurs in conjunction with the southern most latitudinal extension of the equatorial trough, although even during these months the trough remains north of the region. Precipitation in the region, similar to much of the tropics, occurs in showers; therefore, when analyzing rainfall it is better to use a small network of rainfall stations rather than a single station (Riehl, 1979). In this study, we compute normalized departures of rainfall for February through May using a network of stations in the "dry region." A list of rainfall stations used in the indexing appears in Table 1. The method of computing departures is outlined in Kraus (1977) and provides a useful index of regional rainfall for each day. The purpose of creating a rainfall index is two-fold. First, it aids in the time-series analysis of data. Secondly, it is used to help determine days of extreme rainfall for compositing the upper-air information.

We briefly describe the method. Let r_{ij} be the daily rainfall of station i during day j, J be the number of days in the analysis period, and J_i be the number of days with a record at station i during the period J. Also, let I be the number of stations in the region to be analyzed and I_j the number of regional stations in operation on day j. Thus, the mean daily rainfall at station i and its variance are:

$$\bar{r}_i = \frac{1}{J_i}\sum_j r_{ij}, \qquad \sigma_i = \left(\frac{1}{J_i}\sum_j r_{ij}^2 - \bar{r}_i^2\right)^{1/2}.$$

The normalization is $x_{ij} = (r_{ij} - \bar{r}_i)/\sigma_i$ and the area-averaged value of x_{ij} for the day j is $a_j = (1/I_j)\sum_i x_{ij}$. We must first check to see if spatial variations of the x_{ij}'s between different places within the region are small relative to day-to-day variations as a whole (a_j's). To do this we use the F-test or ratio-of-variance test.

Let v_t be the variance in time and v_a be the variance in space. Then

$$v_t = \frac{\sum I_j a_j^2}{J-1}, \qquad v_a = \frac{N - \sum I_j a_j^2}{N-J}$$

where $N = \sum I_j = \sum J_i = 2428$ in this study. For our data then:

variances:

$$v_t = 2.71 \qquad v_a = 0.91$$

degrees of freedom:

$$J - 1 = 119 \qquad N - J = 2308.$$

The ratio of variance (v_t/v_a) estimate is 2.97 which is significant, since the limiting value of F for 1% probability is 1.32. In other words, the probability that the differences between days in the combined regional rainfall record is a result of random fluctuations is less than 1:100.

Table 2 shows both the area-averaged normalized rainfall anomalies (a_j) and the unnormalized area averages ($\bar{x}_j$). From the table we can see that May was the driest of the four months, particularly toward the end of the

Table 2. *Normalized rainfall departures* (a_j) *and area averaged daily rainfall* (*mm*) ($\bar{x}_j$)

February	a_j	$\bar{x}_j$	March	a_j	$\bar{x}_j$	April	a_j	$\bar{x}_j$	May	a_j	$\bar{x}_j$
1	−0.29	0.27	1	−0.31	0.14	1	0.03	3.64	1	0.00	3.29
2	0.74	12.24	2	−0.17	1.05	2	−0.25	0.61	2	−0.04	3.12
3	0.55	8.66	3	−0.32	0.00	3	−0.32	0.00	3	0.23	4.76
4	0.64	11.37	4	−0.06	3.46	4	−0.16	1.76	4	0.37	8.02
5	−0.28	0.63	5	0.45	9.26	5	−0.15	3.11	5	−0.06	1.94
6	−0.02	2.29	6	0.31	5.88	6	−0.19	0.97	6	0.05	2.99
7	0.28	5.05	7	−0.32	0.00	7	0.46	8.70	7	−0.21	1.24
8	0.80	12.98	8	−0.01	2.90	8	0.05	3.74	8	−0.05	1.48
9	0.00	3.71	9	−0.22	0.63	9	0.17	5.85	9	−0.12	1.85
10	−0.21	1.20	10	−0.08	3.45	10	−0.05	4.47	10	−0.31	0.00
11	−0.21	1.20	11	0.05	5.24	11	−0.32	0.00	11	−0.20	1.19
12	0.25	5.75	12	0.19	4.91	12	−0.25	0.67	12	−0.17	1.13
13	−0.09	1.27	13	0.65	13.66	13	−0.05	2.92	13	−0.30	0.22
14	0.02	2.20	14	0.28	5.58	14	−0.29	0.21	14	−0.31	0.04
15	−0.16	1.63	15	0.12	4.47	15	−0.32	0.00	15	−0.31	0.03
16	−0.24	0.68	16	0.37	5.65	16	−0.22	1.01	16	0.06	3.10
17	−0.10	2.21	17	0.08	4.46	17	−0.29	0.36	17	0.16	1.29
18	−0.25	0.62	18	−0.28	0.63	18	−0.29	0.26	18	0.14	3.59
19	−0.23	0.87	19	−0.32	0.00	19	−0.27	0.30	19	0.20	1.14
20	−0.09	2.11	20	−0.12	1.95	20	−0.27	0.36	20	−0.15	0.24
21	0.06	2.64	21	−0.28	0.33	21	0.38	6.47	21	−0.31	0.00
22	−0.32	0.00	22	−0.32	0.00	22	−0.14	1.41	22	−0.26	0.63
23	0.14	3.66	23	−0.32	0.00	23	−0.21	0.42	23	−0.31	0.00
24	0.61	11.69	24	−0.32	0.00	24	1.06	12.65	24	−0.31	0.00
25	0.10	4.39	25	−0.25	0.52	25	0.67	9.45	25	−0.31	0.19
26	0.79	10.15	26	−0.13	3.03	26	1.05	12.86	26	−0.10	1.67
27	0.07	4.52	27	0.23	3.92	27	−0.02	3.54	27	−0.31	0.00
28	−0.30	0.20	28	1.29	14.30	28	0.36	8.66	28	−0.31	0.00
			29	1.47	21.13	29	−0.23	1.35	28	−0.31	0.00
			30	0.21	5.00	30	−0.10	2.12	30	−0.31	0.00
			31	−0.16	2.38				31	−0.31	0.00

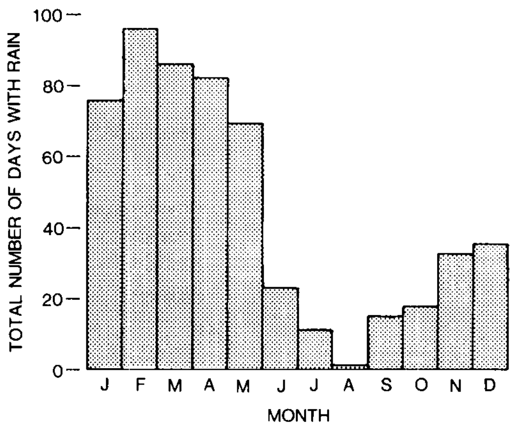

Fig. 3. Histogram of total number of days with rain from stations in the dry region for each month of 1979.

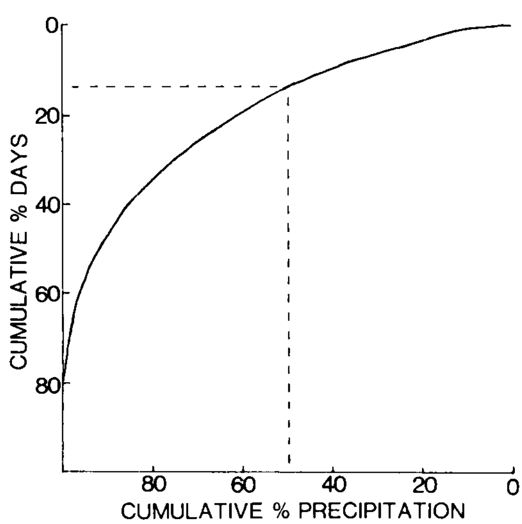

Fig. 4. Graph of cumulative % total regional daily precipitation versus cumulative % days.

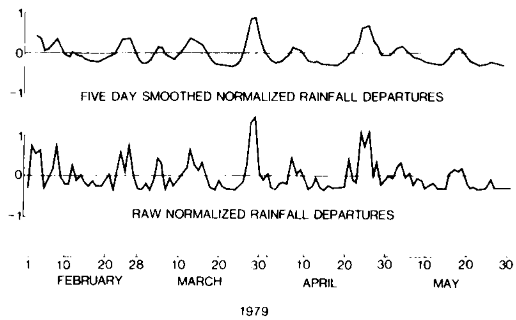

Fig. 5. Graphs of raw and 5-day smoothed normalized rainfall departures for the period February through May of 1979.

month. May had 9 days without any recorded precipitation, while February, March, and April combined had a total of 10 days without rainfall. Even though May is regarded as a transition month the total number of days with rainfall is large enough to regard it as a rainy season month (see Fig. 3). So, the data for May are included in the composites.

Analysis of precipitation concentration reveals the following: 14% of the days with rain during the rainy season account for 51% of the rainfall (Fig. 4), while 31% of the days account for 76%. Conversely, precipitation from 50% of the days with the least rain amounts to only 8% of the total. For compositing purposes we chose the 19 days with no precipitation as the dry composite. Then, for similarity, we picked 19 days with the largest area-averaged normalized precipitation for the wet composite. However, since the three data sets (aerological stations, FGGE-level IIIb grids, and percent bright cloudiness) have different time domains, the number of days for each composite depends on the data set used.

We have shown that area-averaged normalized rainfall departures are not random in time, therefore we employ time-series techniques as a way to further understand physical processes which produce the precipitation. Fig. 5 shows graphs of raw and five-day smoothed normalized departures. Outstanding peaks are noted at the end of March and again at the end of April. May is conspicuous for a tapering of positive rainfall departures, indicating a transition from the wet to dry season. A closer look at the time-series of raw departures reveals that daily variability during February is large compared with the remainder of the rainy season. This indicates a possible trend from short duration showers in the early season to more intense and persistent rainfall systems in the later season. Fig. 6 shows the autocorrelation function of raw normalized rainfall departures. We note a sharp drop in positive correlation for the first several lags, indicating little persistence beyond 2 or 3 days. A peak is noted in the range of 13–16 days.

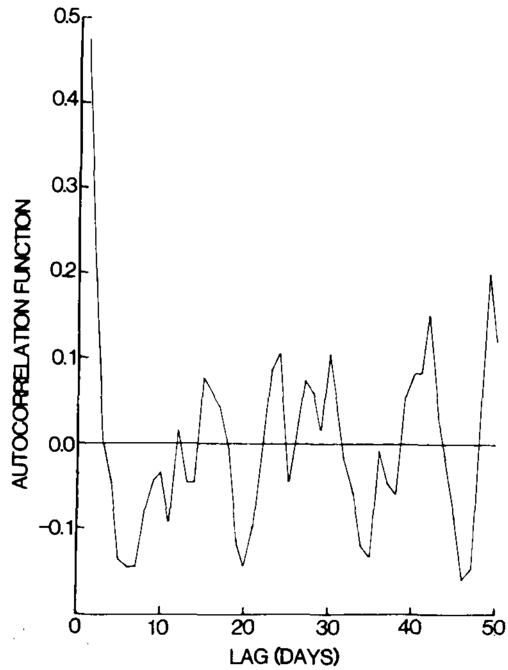

Fig. 6. Correlogram of raw normalized rainfall departures.

4. Horizontal wind

Vertical cross-sections of zonal wind are plotted for both wet and dry composites. Data are from the FGGE-level IIIb grids and therefore only the months of March and April are included. Analyses were subjected to a 25-point smoothing filter. The cross-section which slices the cylinder roughly in half along the 41°15′ meridian is shown in Fig. 7a, b.

One of the most striking differences between composites is the relative strength of low- and mid-level easterlies during dry days. This finding is nearly identical to findings from studies of interannual and seasonal variations (Hastenrath and Heller 1977; Marques et al. 1983), etc. Riehl (1979) remarked about the lack of a wind discontinuity at the trade wind inversion base. Strong easterlies during dry days at low levels suggest strong trade-wind subsidence at middle and high levels over the region.

A plot of upper-level horizontal wind vectors averaged over three vertical levels (150, 200, 250 mbs) is shown in Fig. 8a, b. Clearly depicted is a vortex north of northeast Brazil during dry days and an extension of the western South Atlantic trough into the region during wet days. The vortex is absent during wet days. The trough over the western South Atlantic near 35° W may allow for equatorward advancing midlatitude cold frontal systems described by Kousky (1979). According to Kousky (1985), a frontal system enhances convergence and therefore helps organize convective activity over Brazil. During dry days the vortex north of Brazil inhibits the development of a trough as far south as northeastern Brazil. Cyclonic vortices near northeast Brazil

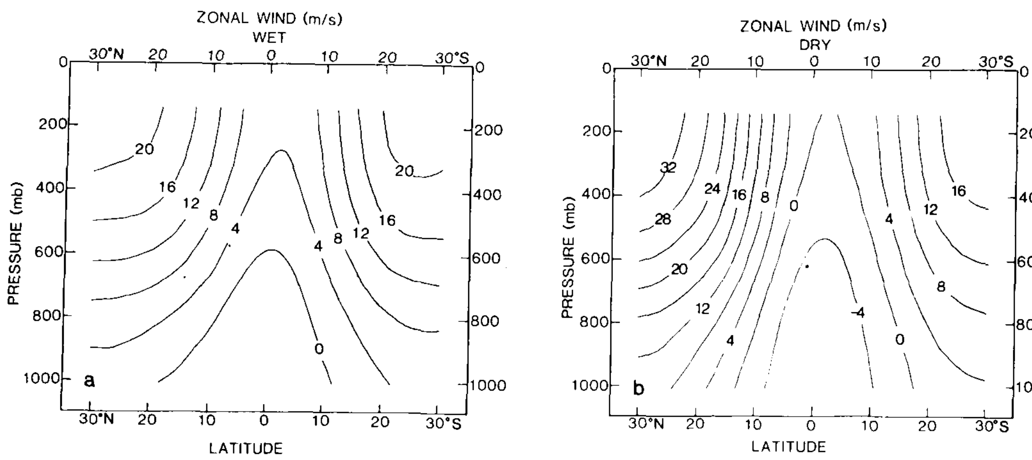

Fig. 7. Vertical cross sections of zonal wind along the longitude 41°15′W for wet (a) and dry (b) composites.

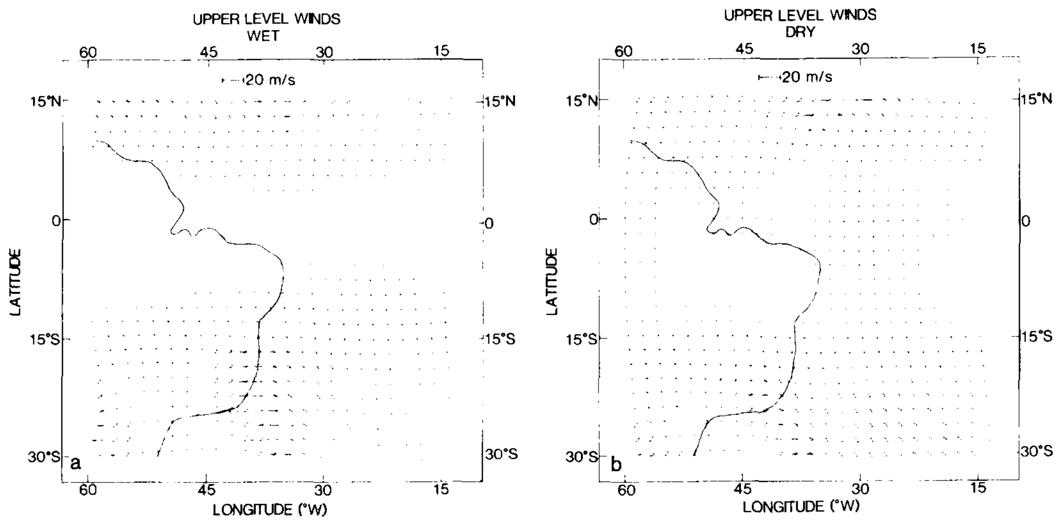

Fig. 8. Upper tropospheric horizontal winds averaged over 150, 200 and 250 mb for wet (a) and dry (b) composites. Lengths of vectors are proportional to speed.

during the rainy season have been documented by Kousky and Gan (1981).

Lag-cross correlations were computed between rainfall departures and relative vorticity. Upper-level cyclonic vorticity was negatively correlated with rainfall, particularly around minus one lag, as was expected. Positive correlations appear around minus seven lag. Coefficients are near 0.55. Low-level anticyclonic vorticity showed no large correlations with rainfall.

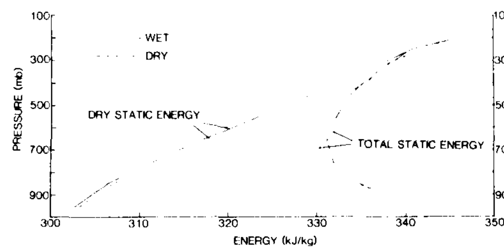

Fig. 9. Averaged vertical profiles of total and dry static energies for both composites.

5. Thermodynamic energy content of the cylinder

The horizontal surfaces of the cylinder are divided into a grid with 9 points equally spaced around the perimeter and one center point. The diameter of the cylinder is approximately 1400km. Distance between points on the perimeter is nearly 500km. This cylinder is slightly larger than the one used by Marques et al. (1983). The vertical is divided into nine levels with an equal separation of 100 mb from 1000 to 100 mb. Vertical-space sections are constructed and analyzed for each parameter, with pressure on a linear scale as the ordinate, and the circumference distance as the abscissa. Grid values are picked up at each grid point for all levels. Thermodynamic energy components are then computed before averaging horizontally to yield mean values around the cylinder for each level. Layered averaged values are used in the discussion. Energy values are also computed for the centered grid point.

Table 3 displays the values of energy content for the atmosphere over northeast Brazil during wet and dry days, and for the center grid for both composites. For both wet and dry composites, we see a minimum in total thermodynamic energy in the middle troposphere (Fig. 9). According to Riehl (1979), this is typical of the tropical atmosphere.

From vertical profiles of moist static energy, some interesting observations can be made. In

Table 3. *Mean thermodynamic energy of the atmosphere (kJ/kg)*

Pressure layer (mb)	C_pT	ϕ	Lq	$C_pT+\phi$	Total
		a. Cylinder wet			
SFC–900	297.2	5.5	39.2	302.7	341.9
900–800	291.4	15.0	28.4	306.4	334.8
800–700	286.1	25.4	20.2	311.6	331.8
700–600	280.3	37.1	13.8	317.4	331.1
600–500	273.1	50.4	8.6	323.5	332.1
500–400	263.3	66.1	4.3	329.4	333.7
400–300	250.3	84.8	1.5	335.1	336.6
300–200	232.0	108.5	0.0	340.5	340.5
200–100	208.9	142.3	0.0	351.2	351.2
		b. Cylinder dry			
SFC–900	297.7	5.6	38.6	303.2	341.9
900–800	291.9	15.0	27.6	306.9	334.5
800–700	286.8	25.5	18.3	312.3	330.5
700–600	281.0	37.1	11.5	318.1	329.6
600–500	273.7	50.5	6.5	324.1	330.7
500–400	264.2	66.2	3.0	330.4	333.4
400–300	251.0	84.9	1.1	336.0	338.0
300–200	232.3	108.8	0.0	341.1	341.1
200–100	208.1	142.7	0.0	350.8	350.8
		c. Center grid wet			
SFC–900	999.9	999.9	999.9	999.9	999.9
900–800	999.9	999.9	999.9	999.9	999.9
800–700	288.5	25.6	25.3	314.1	339.4
700–600	282.3	37.3	16.9	319.7	336.5
600–500	274.9	50.8	9.8	325.6	335.4
500–400	265.5	66.6	4.7	332.0	336.8
400–300	253.0	85.3	1.4	338.2	339.6
300–200	234.2	109.0	0.0	343.2	343.2
200–100	211.5	143.1	0.0	354.6	354.6
		d. Center grid dry			
SFC–900	999.9	999.9	999.9	999.9	999.9
900–800	999.9	999.9	999.9	999.9	999.9
800–700	287.7	25.7	13.8	313.4	327.1
700–600	282.1	37.3	5.8	319.5	325.2
600–500	274.8	50.7	2.2	325.5	327.7
500–400	265.0	66.4	1.6	331.5	333.1
400–300	251.8	85.2	1.5	337.0	338.5
300–200	233.6	109.1	0.0	342.7	342.7
200–100	209.0	143.2	0.0	352.2	352.2

the lowest layer, total energies are the same for wet and dry composites. Wet days have more latent heat but less sensible heat, while dry days have more sensible heat but less latent heat. Between 400 and 900 mb, the effect of greater latent heat offsets the sensible heat, resulting in larger total energies during wet days. Between 200 and 400 mb, the latent energy vanishes and the effect of sensible heat dominates, producing larger total energy values during dry days. Further, between 100 and 200 mb, sensible heat is greatest during wet days, resulting in larger total energy in the upper troposphere. These profiles are similar to Marques et al. (1983) for wet and dry years, but the present values are slightly smaller at all levels. Possible explanations for these profiles include stronger mid-tropospheric subsidence warming during dry days, indicating the proximity of the South Atlantic high (SAH). Stronger undiluted cumulonimbus transports lower tropospheric heat to the upper layers during wet days. And stronger cumulus transports latent heat to low and middle tropospheres during wet days.

For the center grid, we find large differences in total energy between composites, with wet days having significantly more total energy than dry days particularly in the middle troposphere (Fig. 10). We also note that the minimum energy layer during wet days is the 500–600 mb layer, while for dry days it is the 600–700 mb layer. These results suggest more extensive cumulus transport during wet days.

6. Normal component of velocity

Fig. 11 shows normal velocity profiles and error bars for both wet and dry composites. Error limits are computed using standard deviations of wind speed and direction provided by Fuelberg and Scoggins (1980). The error bars are quite large in the mid-troposphere. Positive values indicating an inward component are found at nearly all levels and for both composites. Largest differences appear in the mid-troposphere. During dry days a stronger inward component translates to stronger convergence and implied stronger subsidence below. This is in contrast to wet days near 500 mb where the normal velocity is close to zero. However, as noted above, random wind errors in the aerological reports result in largest normal velocity variance in the mid-troposphere.

Mass adjusted wind divergence in each layer of the cylinder is estimated using the formula, $D = (S/A)V_n$, where S is the circumference of the cylinder, A is the area and V_n is the mass-adjusted normal velocity component. Vertical motions are then computed using the kinematic method. Wet days have a composite mass-adjusted upward motion throughout the troposphere, with dry days showing sinking motions. Fig. 12a, b show a composite of % bright (cold) cloud amount for wet and dry days for the months of February through April. As expected, large-scale descending motions of the dry days over Nordeste agree well with the low percentage of bright cloudiness in the region. We note that during wet days the intertropical cloud band has

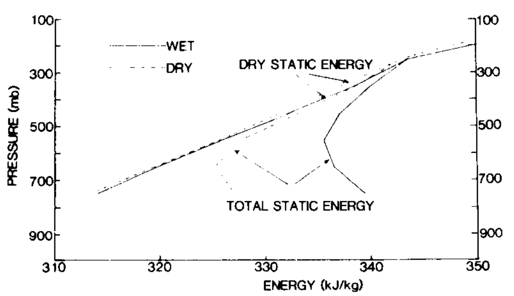

Fig. 10. Same as Fig. 9 except at center grid only.

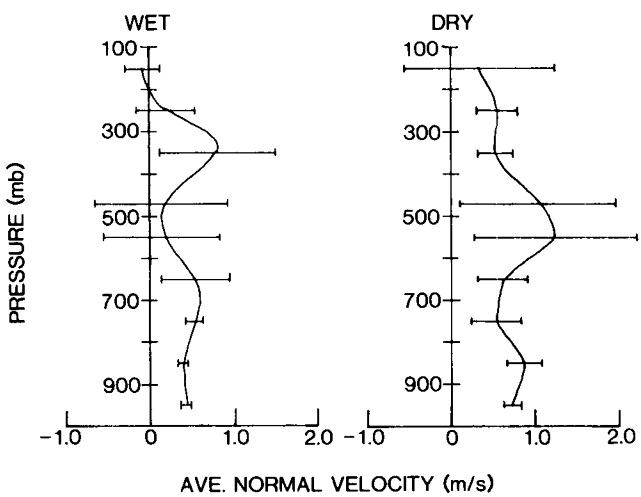

Fig. 11. Vertical profiles of averaged normal velocities for both composites including error bars.

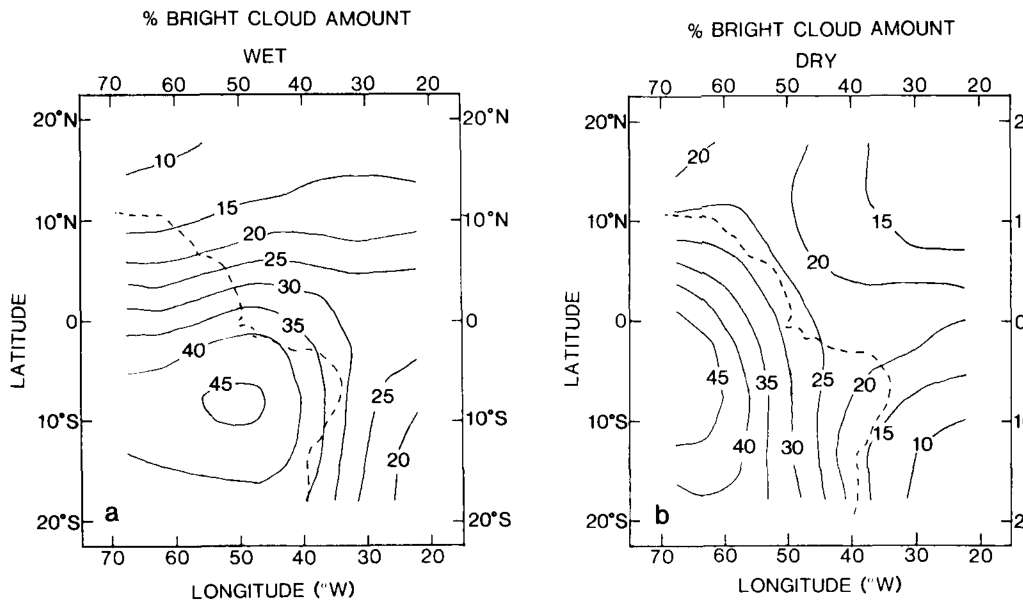

Fig. 12. Composite bright cloud amount for wet (a) and dry (b) days.

a considerably larger meridional extent. Further we note an eastward shift of bright cloudiness from dry to wet days. This shift is a result of weakened subsidence over northeast Brazil. Large-scale subsidence dominates the region of northeast Brazil, however, with an equatorward advancement of an upper-level trough low-level frontal intrusions occur, enhancing convergence and weakening the subsidence. Kousky (1979) has noted an eastward shift of rainfall over Brazil as a result of southern hemispheric frontal intrusions. As a consequence of these fronts a low-level wind shift from the southeast to the north or northwest occurs (Kousky, 1985). We have similarly noted a relative weakening of the low-level easterlies during wet days (see Section 4).

7. Heat and moisture fluxes

Sensible and latent heat fluxes have been evaluated at each boundary grid and for the cylinder as a whole. The equations used were developed in Marques et al. (1983) and are shown here for convenience.

$$\mathrm{SHF} = \frac{R}{g}\int_{p_t}^{p_0} (C_p\, T + \phi) V_n \, \mathrm{d}p \qquad \text{and}$$

$$\mathrm{LHF} = \frac{R}{g}\int_{p_t}^{p_0} Lq\, V_n \, \mathrm{d}p$$

where

$\mathrm{d}p$: is the vertical layer = 100 mb,
V_n : is the normal component of horizontal velocity (m/s),
$C_p\, T + \phi$: is the sensible heat (kJ/kg),
R : is the radius of the cylinder ~ 700 km,
g : is acceleration due to gravity = 9.8 m/s^2,
Lq : is the latent heat (kJ/kg).

For the cylinder as a whole, these equations are integrated along the boundary. Flux values are also computed at each boundary grid.

Table 4 shows flux directions of $C_p\, T + \phi$ and $C_p\, T + \phi + Lq$ for both composites. The magnitude of wind errors allows only for a meaningful comparison of flux direction. During wet days we find an inward flux of sensible heat in low layers (below 600 mb) with a net export above. In contrast, during dry days we find a net export below 600 mb with a net import above. Inward fluxes of sensible heat are found only during wet days at lower levels. Fluxes of water vapor are comparatively weak. However, we find a low-

Table 4. *Mean thermodynamic energy flux direction*

Pressure layer (mb)	$C_pT + \phi$	Lq	Total
	a. Cylinder wet		
SFC–600	+	+	+
600–100	–	–	–
	b. Cylinder dry		
SFC–600	–	–	–
600–100	+	–	+

level inward moisture flux below 600 mb during wet days with a net export during dry days. In addition to increased convergence associated with surface fronts, a wind shift in advance of the front to a more northerly direction allows for a greater moisture flux into the region.

We divided the cylinder approximately in half from northeast to southwest and totalled the moisture flux across the northwest and southeast halves of the cylinder. Results indicate a moisture flux into the cylinder from the northwest and a slightly weaker outflux of moisture from the southeast. Direction of flux is almost the same for both wet and dry composites. During wet days the region receives approximately 17% more moist energy than during dry days. Again, however, considering the wind errors, the significance may be only that the wet days receive more moist energy than the dry days.

8. Summary and conclusions

Daily variability of rainfall, horizontal wind and thermodynamic energies over northeast Brazil have been examined for the rainy season of 1979. We have found that there are significant differences between wet and dry days over the region.

Rainfall was analyzed by indexing daily totals from stations in a specific "dry region" over a portion of northeast Brazil. We found that, in the region as a whole, daily fluctuations were not random. Applying time-series techniques to rainfall data we noted a peak in the 13–16 day range. May appeared to be a transition month between the well defined wet and dry seasons, even though the total number of rainfall days indicated a wet season month.

Vertical cross-sections of zonal wind revealed stronger low- and middle-level easterlies during dry days with stronger upper-level westerlies south of the equator during wet days. Analysis of wind vectors averaged for three tropospheric levels indicated the existence of an upper-level vortex during dry days and a stronger trough over the western South Atlantic during wet days. Averaged normal velocities implied low-level convergence and upper-level divergence during wet days. A reversal of this pattern was noted during dry days. Averaged speeds were small, as can be expected on this scale.

Comparatively large values of sensible heat in upper levels and larger latent heat in low and middle levels during wet days led us to conclude that there was an increase in cumulus and cumulonimbus transports during this time. Also we detected a low-level influx of moisture to the region during wet days, while a weak export of moisture of low levels was noted during dry days. The strongest inward-moist energy fluxes were found along the northwest half of the cylinder for both wet and dry days. Possible moisture sources were the Amazon basin and the equatorial trough.

From analysis of results it appeared that rainfall on a daily basis was related to the strength of subsidence over the region, which inhibited growth of cumulus and cumulonimbus transports. This in turn was controlled by the existence of upper-level troughs and vortices. When a trough over the western South Atlantic extended over portions of northeast Brazil low-level easterlies were weaker and rainfall was enhanced. Kousky (1985) showed that associated with enhanced troughing was a southeastward displacement of the 850 mb anticyclone and consequently a weakening of the southeasterly low-level trades. These circulation changes accompanied the equatorward advancements of southern cold fronts. The increased moisture flux from the north noted during wet days in this study gives some indication of these fronts. Further during dry days the vortex north of the region acted as a block prohibiting the northward advancements of the troughs.

It would be worthwhile to repeat this investigation for several years, including years of extreme drought and extreme rainfall.

9. Acknowledgements

The authors wish to thank anonymous reviewers for their constructive criticisms. Also special thanks to Margaret Kleiber for typing the manuscript and Bill Lueders for editing. This work was supported by the Space and Science Applications office, National Aeronautics and Space Administration under grant no. NAG 5-384. A partial support for graduate students and computer usage came from the Graduate School.

REFERENCES

Fuelberg, H. E. Scoggins, J. R. 1980. Kinetic energy budget during strong jet stream activity over the eastern United States. *Mon. Wea. Rev. 108*, 69–77.

Hastenrath, S. and Heller, L. 1977. Dynamics of climatic hazards in northeast Brazil. *Q. J. R. Meteorol. Soc. 103*, 77–92.

Kousky, V. E. 1979. Frontal influences on northeast Brazil. *Mon. Wea. Rev. 107*, 1140–1153.

Kousky, V. E. 1985. Atmospheric circulation changes associated with rainfall anomalies over tropical Brazil. *Mon. Wea. Rev. 113*, 1951–1957.

Kousky, V. E. and Gan, M. A. 1981. Upper tropospheric cyclonic vortices in the tropical South Atlantic. *Tellus 33*, 538–551.

Kraus, E. B. 1977. Subtropical droughts and cross-equatorial energy transports. *Mon. Wea. Rev. 105*, 1009–1018.

Marques, V. S., Rao, B. and Molion, L. C. B. 1983. Inter-annual and seasonal variations in the structure and energetics of the atmosphere over NE Brazil. *Tellus 35A*, 136–148.

Moura, A. D. and Shukla, J. 1981. On the dynamics of droughts in NE Brazil: Observations, theory and numerical experiments with a general circulation model. *J. Atmos. Sci. 38*, 2653–2675.

Ramos, R. P. L. 1975. Precipitation characteristics in Northeast Brazil. *J. Geophys. Res. 80*, 1665–1678.

Riehl, H. 1979. *Climate and weather in the tropics.* Academic Press, New York.

Strang, D. M. D. 1972. Climatological analysis of rainfall normals in northeastern Brazil. *Pap. IAE-M-02/72*, 70 pp., Centro Tecnico Aerospacial, Sao Jose dos Campos, Brazil, 1972.